Orographic Influences on an Oahu Flood

MICHAEL J. MURPHY JR.* AND STEVEN BUSINGER

School of Ocean and Earth Science and Technology, University of Hawaii at Manoa, Honolulu, Hawaii

(Manuscript received 26 January 2010, in final form 10 November 2010)

ABSTRACT

On 2 April 2006, Oahu's Koʻolau Mountain Range endured more than 6 h of heavy rain with accompanying flash flooding along its northeast-facing slopes. The storm responsible for the event left a pattern of precipitation characteristic of orographic anchoring of convection with extreme rainfall gradients along the slopes and maxima along the crest of the mountain range. In fact, this was the third flash-flood event to impact the Koʻolau Mountains in just over 1 month, with each event occurring under conditions of moist southeasterly flow at low levels and moderate conditional instability. Under these conditions persistent convection and localized heavy rainfall often occur over the Koʻolau Mountain Range. Mesoscale analyses of the thunderstorm complex responsible for the 2 April 2006 heavy rain event and the results of a high-resolution numerical simulation employing the Weather Research and Forecasting (WRF) model are described in this study.

Key features of the convection that contributed to the longevity of the event include repeat formation of convective cells along the eastern side of the central Koʻolaus, minimal horizontal cloud motion, and strong updrafts that sloped toward the northwest in the lower levels. The westerly shear of the low-level flow determined the pattern of accumulated precipitation by aligning the slope of the convective updrafts nearly parallel to the southeast-to-northwest-orientated Koʻolau Mountain Range. The microphysical structure of the convection was complex, with the vertical advection of hydrometeors originating below the freezing level facilitating high concentrations of ice particles and an environment conducive to charge separation and lightning.

1. Introduction

A series of deep convective cells formed over Oahu's Koʻolau Mountain Range (Fig. 1) on 2 April 2006, leading to a quasi-stationary thunderstorm complex that persisted for over 6 h. Ensuing flash floods in many of the northeast-facing watersheds of eastern Oahu caused a road closure and precautionary evacuations. The event exhibited a pattern of precipitation with extreme gradients and rainfall totals of over 225 mm recorded by gauges along the crest of the Koʻolaus.

The Oahu flash flood occurred at the end of an exceptionally wet period in the Hawaiian Islands that began in mid-February 2006 (Nash et al. 2009). This extended wet period saw a prolonged synoptic blocking pattern over the North Pacific and the formation of numerous low pressure systems to the west of the state. Heavy rainfall occurred throughout the island chain with record-setting amounts measured by gauges on the islands of Kauai and Oahu, and seven deaths resulting from the breaching of Kauai's Ka Loko Dam on 14 March. Of the many heavy rain events that occurred on Oahu during this period, three cases were accompanied by southeast low-level flow and a pattern of precipitation with extreme gradients and maxima concentrated along the crest of the Koʻolaus (Figs. 2 and 3). Patterns of precipitation of this type are not unique to the spring 2006 wet period; in fact, they are often found on Oahu in association with southeasterly low-level flow (K. Kodama, NWSFO-HFO, 2008, personal communication).

Heavy rain events present a significant hazard to the Hawaiian Islands and have proven challenging to forecast (Kodama and Businger 1998). Lack of in situ observations combined with mountainous terrain and small watersheds with rapid response times make prediction of flash floods especially difficult (Blumenstock and

* Current affiliation: Hydrologic Research Center, San Diego, California.

Corresponding author address: Steven Businger, Dept. of Meteorology, University of Hawaii at Manoa, 2525 Correa Rd., Honolulu, HI 96822.
E-mail: businger@hawaii.edu

DOI: 10.1175/2010MWR3357.1

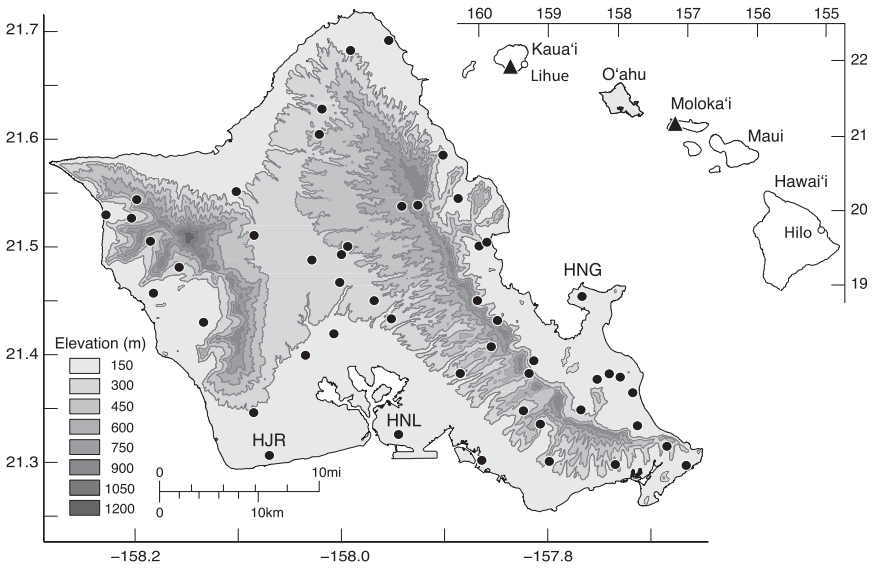

FIG. 1. Terrain map of the island of Oahu with elevation shaded. The Ko'olau Mountain Range runs along the eastern coastline with the Waianae Mountain Range in the western parts of the island. Dots represent locations of surface observing stations with the first-order stations at the HNL, HNG, and HJR airports labeled. Inset shows a map of the Hawaiian Islands with the locations of the HKI and HMO radar stations, on the islands of Kauai and Molokai, respectively, indicated by triangles. The Hilo and Lihue rawinsonde sites are also indicated. [Here and in other figures, the vertical and horizontal axes are labeled with latitude (°N) and longitude (°W), respectively].

Price 1967; Schroeder 1977). One of the earliest studies on flooding events in Hawaii was performed by Haraguchi (1977). His study examined 11 heavy rain events on Kauai, Oahu, and Maui with 24-h rainfall totals ranging between 150 and 521 mm. All of the events occurred under one of four general synoptic situations: 1) kona storms, 2) cold fronts–shearlines, 3) upper-level troughs, or 4) tropical systems. The events were found to have 1) maximum rainfall on slopes facing the low-level winds, 2) been associated with thunderstorms, 3) had a 500-mb trough to the west of the islands, and 4) occurred mostly at night. Haraguchi also noted that Oahu was especially prone to severe local flooding.

Maddox et al. (1979) investigated 151 heavy rain events in the continental United States and found eight common features: 1) presence of convective storms, 2) high surface dewpoints, 3) high moisture content throughout a deep tropospheric layer, 4) weak to moderate vertical wind shear through cloud depth, 5) convective clouds that repeatedly form and move over the same area, 6) a large-scale 500-mb ridge in the vicinity, 7) a midlevel short wave moving along the ridge, and 8) heaviest rainfall occurring at night.

These results agree well with studies of Hawaiian heavy rain events with the following notable differences. 1) Several Hawaiian case studies (Schroeder 1978; Cram and Tatum 1979; Dracup et al. 1991) found that flash floods have occurred without the presence of thunderstorms. Hawaiian precipitation systems with cloud tops below the freezing level have produced instantaneous rainfall rates greater than 250 mm h^{-1} (Fullerton and Wilson 1975). 2) A study of the 1987 New Year's Eve flood on Oahu by Dracup et al. (1991) found strong vertical wind shear present.

Kodama and Barnes (1997) studied 44 heavy rain events over the southeast slopes of Mauna Loa on Hawaii Island. They found that rainfall was positively correlated with the strength of the upslope component of the low-level flow and the amount of midlevel moisture. All of the events occurred under one of the four general synoptic situations identified by Haraguchi (1977). In each case the vertical motion associated with the synoptic disturbance eroded the trade wind inversion and the environmental air at midlevels moistened considerably. Among the stability indices, the *K* index (George 1960) was found to be the most useful predictor of heavy rain in these situations. The authors suggested that a moist midlevel environment facilitates heavy rain by reducing dry air entrainment into clouds. This can result in more vigorous convection while also suppressing downdrafts, which can stabilize the low-level environment or trigger propagation of a system away from its genesis region by forcing conditionally unstable air around the storm upward (e.g., Newton 1966).

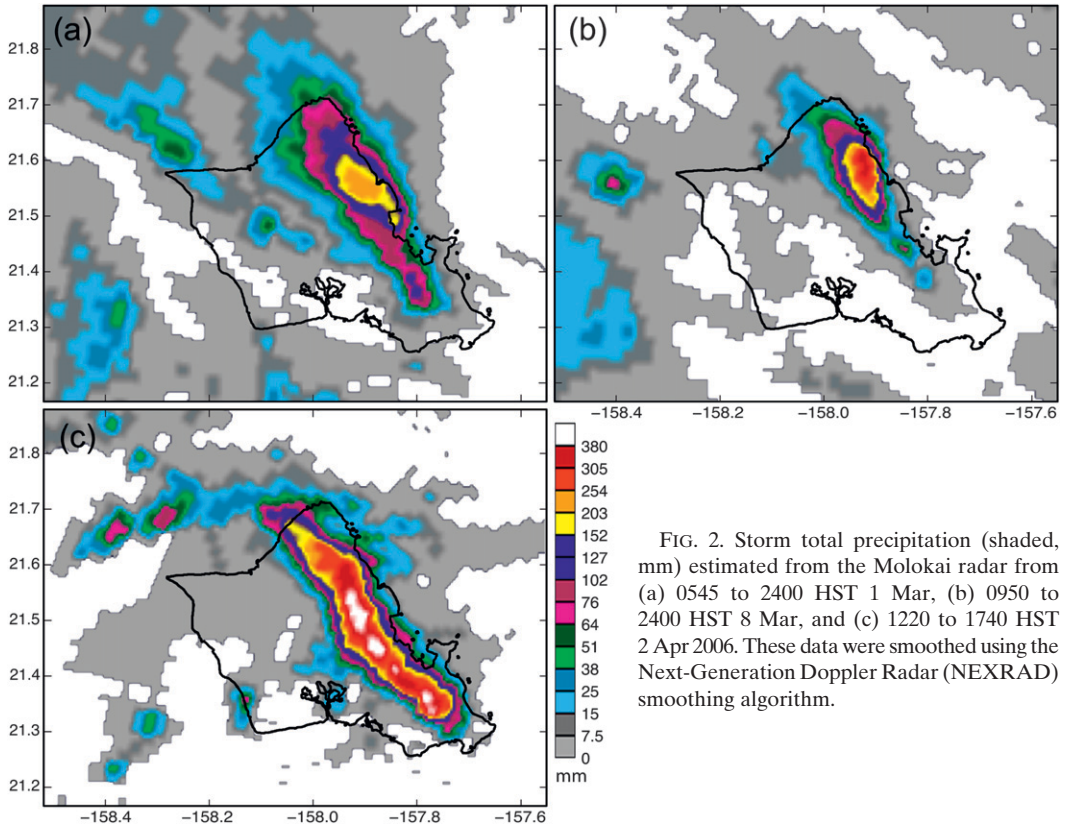

FIG. 2. Storm total precipitation (shaded, mm) estimated from the Molokai radar from (a) 0545 to 2400 HST 1 Mar, (b) 0950 to 2400 HST 8 Mar, and (c) 1220 to 1740 HST 2 Apr 2006. These data were smoothed using the Next-Generation Doppler Radar (NEXRAD) smoothing algorithm.

Numerous studies have investigated the characteristics of long-lived convective systems. One such system is the squall line, which consists of line-orientated precipitating cumulus convection that is generally observed to last for several hours. Tropical squall lines are observed to form in an environment with strong vertical shear of the horizontal wind at low levels and weaker reversed shear at midlevels (e.g., Barnes and Sieckman 1984; Frank 1978). Analyses of numerically simulated squall lines by Rotunno et al. (1988) found the main factor in system longevity to be the interaction of the low-level shear with the precipitation-induced cold pool. This shear–cold pool interaction enhances the formation of new convective cells and results in an updraft structure that tilts in the low levels. In general, conditions of strong low-level shear with weak winds aloft are associated with the longevity of convective systems and have also been observed in long-lived and quasi-stationary systems over complex orography (e.g., Caracena et al. 1979; Nair et al. 1997; Petersen et al. 1999).

Mesoscale studies of flooding events in complex terrain have led to theories of orographic thunderstorm structure. Schroeder (1977) performed a detailed investigation of a flash flood on Oahu that occurred under the influence of an upper-level trough with moderate easterly winds at low levels. Schroeder determined that the orography of the Ko‘olaus provided anchoring for the cumulonimbus with the rain with the highest intensity falling approximately 8 km west of the Ko‘olau Mountain crest. The anchoring mechanism is driven by moist low-level flow being force lifted by topography to its level of free convection, initiating buoyant ascent. If the orientation of the low-level winds and moisture flux remain unchanged, the orography can generate a stationary area of convective development. Effective separation of convective downdrafts from the low-level updraft combined with the presence of weak winds aloft can help generate a quasi-stationary storm system.

Akaeda et al. (1995) investigated a flash flood that occurred during the Taiwan Area Mesoscale Experiment. Under weak large-scale forcing, convective cells repeatedly formed in the foothills in the lee of Taiwan’s Central Mountain Range, leading to a long-lived mesoscale convective system. A numerical simulation of the event produced a persistent quasi-stationary area of surface convergence near the observed location of the flash flooding. The authors concluded that this area of convergence was generated by a combination of surface heating and the interaction of the large-scale flow with the orography of the island and that this convergence caused the repeated formation of convective cells.

Lyman et al. (2005) studied a heavy rain event in northeastern Maui utilizing full radar volume data from

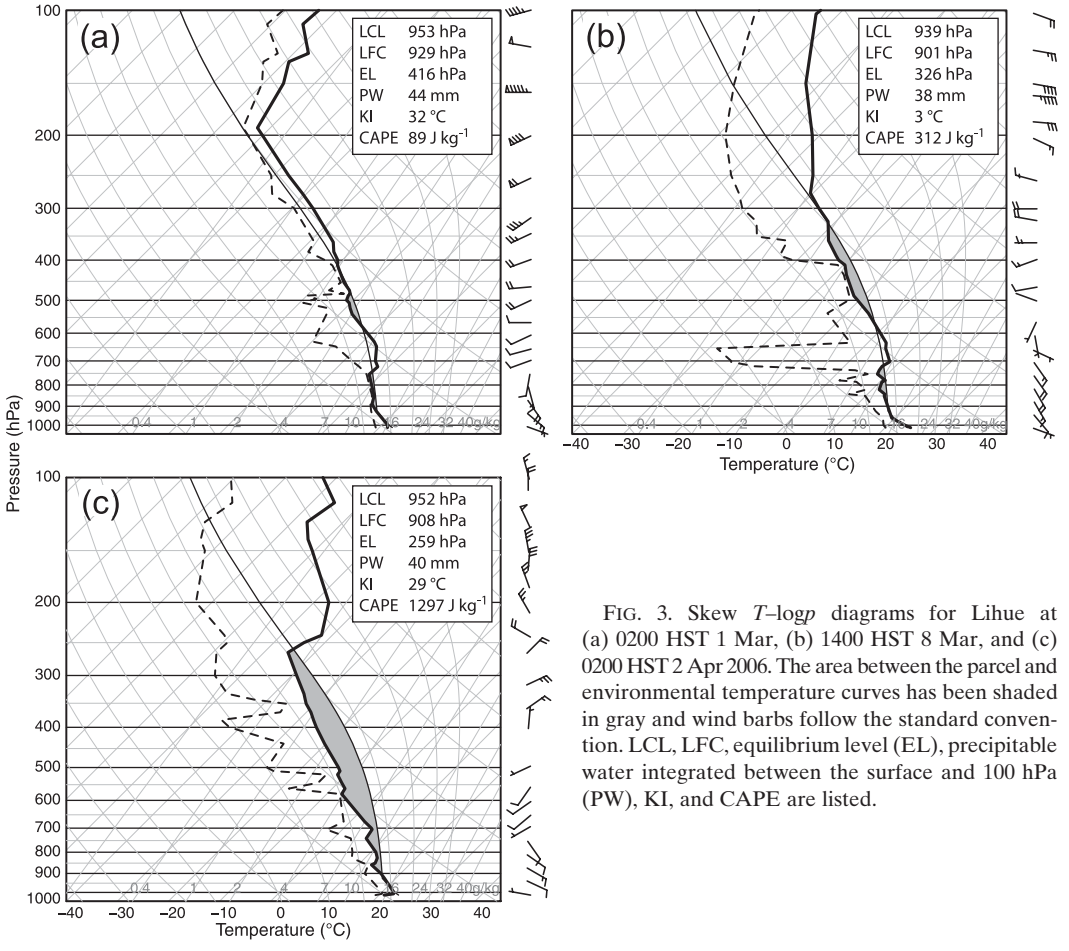

FIG. 3. Skew *T*–log*p* diagrams for Lihue at (a) 0200 HST 1 Mar, (b) 1400 HST 8 Mar, and (c) 0200 HST 2 Apr 2006. The area between the parcel and environmental temperature curves has been shaded in gray and wind barbs follow the standard convention. LCL, LFC, equilibrium level (EL), precipitable water integrated between the surface and 100 hPa (PW), KI, and CAPE are listed.

the Weather Surveillance Radar-1988 Doppler (WSR-88D). Under southeasterly flow at low levels a series of convective cells formed on the southeastern side of the island and followed similar tracks northward. Over 700 mm of rain fell within a period of 7 h in Hana, the main population center of northeastern Maui. The longevity of the event was related to the fact that the low-level outflows of the mature cells were separated from the genesis region by the eastern ridge of the Haleakala volcano. Mesoscale simulations employing the Regional Spectral Model grossly underestimated the observed rainfall in eastern Maui; however, the simulations supported the authors' speculation that the interaction of the low-level flow with Hawaii Island's barrier effect and Maui's topography created enhanced upslope flow over a small zone in eastern Maui.

In the following discussion we present a case study of the 2 April 2006 flooding event on Oahu. The thunderstorm complex responsible for the event is examined with the available observations and simulations employing the Weather Research Forecasting (WRF) model. The goals of this work are to investigate the interaction of moist southeasterly flow with the complex orography of Oahu, identify the basic dynamics of the thunderstorm complex, and explain the convective processes that resulted in the observed pattern of precipitation with respect to the orography.

2. Observations and analyses

a. Geography and meteorological data sources

The Ko'olau Mountain Range runs parallel to the eastern coast of Oahu for approximately 60 km with an average width of 21 km (Fig. 1). These mountains are the remains of single basaltic shield volcano whose northeastern half has almost completely eroded away (Macdonald et al. 1983). The resulting geometry of the mountain range is characterized by a steep eastern scarp, narrow mountain crest, gradually rising western slopes, and a horizontally concave, crescent shape in the southeastern part of the range. Numerous watersheds with steep slopes and narrow basins combined with the island's thin soils make the eastern slopes of the Ko'olaus particularly flood prone (Wang et al. 1970).

Oahu has numerous surface observing stations (Fig. 1). Full surface observations are taken by weather observers stationed at the Honolulu International (HNL), Kaneohe Bay Marine Corps Airfield (HNG), and Kalaeloa (HJR) airports. Limited surface observations (temperature, dewpoint temperature, wind speed and direction, and accumulated precipitation) are also taken hourly at Remote Automated Weather Stations (RAWS) at various locations around the island. Rain gauge data with a temporal resolution of 15 min were obtained from the statewide network of telemetered recording rain gauges, called Hydronet, and also from gauges run by the U.S. Geological Survey, and several quality checked cooperative observing stations. Rawinsondes are normally launched from Lihue and Hilo at 0200 and 1400 Hawaiian standard time (HST = UTC − 10 h); however, the second of the daily launches from Lihue on 2 April 2006 was 3 h late.

Archival radar images (commonly called level III radar data) generated from data taken by the WSR-88D radars on the islands of Molokai (HMO) and Kauai (HKI) (marked on Fig. 1) were examined. These data include base and composite reflectivity, echo tops, and storm total precipitation (STP). The STP is a radar estimate of accumulated rainfall since the last 1-h break in precipitation. Full radar volume data (commonly called level II radar data) are unavailable.

The *Geostationary Operational Environmental Satellite-10* (*GOES-10*) standard visible, infrared, and water vapor channel imagery were utilized, along with the Quick Scatterometer (QuikSCAT) derived near-surface ocean winds. These wind data are available only over the open ocean at a horizontal resolution of 12.5 km and have the limitation of less accurate wind estimation in areas of active precipitation. Synoptic features were identified using the National Centers for Environmental Prediction–National Center for Atmospheric Research (NCEP–NCAR) reanalysis dataset, which has 6-h temporal and 2.5° horizontal resolutions. Finally, lightning data from the Pacific Lightning Detection Network were examined. This network detects cloud to ground lightning strikes with a detection accuracy of approximately 50% and has a location accuracy near Oahu of approximately 16 km (Pessi et al. 2009).

b. Synoptic analyses

The synoptic-scale environment on 2 April 2006 was quite different from the normal Hawaiian trade wind weather. NCEP–NCAR reanalysis charts for 0800 HST show an upper-level trough extending over the state from the northeast with the trough being most pronounced at 500 hPa (Fig. 4a), where a weak closed low in the isoheights is centered over the western end of the state. This disturbance at midlevels is the remnant of a midlevel cutoff low that had been in the vicinity of the Hawaiian Islands over the previous 3 days. The midlevel atmospheric environment over Oahu is characterized by a weak pressure gradient and cold temperatures at midlevels. Destabilization of the atmosphere caused by an upper-level disturbance is a common trigger for deep convection in Hawaii (Haraguchi 1977; Kodama and Barnes 1997). The QuikSCAT satellite passed over the islands just after 0600 HST and revealed moderate easterlies (5–10 m s^{-1}) over the waters near the state (Fig. 5). As the day progressed, the midlevel disturbance drifted slowly toward the east and weakened.

Rawinsonde launches from Lihue and Hilo at 0200 HST (Figs. 3c and 6, locations indicated in Fig. 1) indicated weaker midlevel winds and a much moister midlevel environment over Lihue. The synoptic-scale ascent associated with the trough aloft eliminated the trade wind inversion over the western end of the state (e.g., Kodama and Barnes 1997) while only a thin isothermal layer remained over Hilo. Both environmental soundings display midlevel temperatures below −10°C, indicating the potential for a rising air parcel to maintain positive buoyancy high into the atmosphere. The convective available potential energy (CAPE) values of 1014 and 1297 J kg^{-1} at Hilo and Lihue, respectively, are high for the Hawaiian Islands; the average CAPE value for the events studied by Kodama and Barnes (1997) was only 452 J kg^{-1}. The *K* index (KI) value of 29 in the Lihue sounding is suggestive of low-end moderate convective potential; all of the flooding events studied by Kodama and Barnes (1997) had KI values of 30 or greater. Very little convective inhibition is present in the Lihue sounding. The lowest layer in this sounding is conditionally unstable, with calculations—using parcel method thermodynamics—predicting that lifting of this surface air up to the 900-hPa level (the level of free convection), will result in buoyant ascent.

The Lihue sounding was used to assess the environmental conditions near the Ko‘olaus despite the possible error introduced by its distance of approximately 130 km from Oahu. This sounding shows light to moderate easterlies throughout the lower troposphere with the mean winds in the lowest 300 hPa at approximately 6 m s^{-1} from the southeast. Low-level southeast flow has been a common feature in many Hawaiian heavy rain events (e.g., Kodama and Barnes 1997; Lyman et al. 2005). Above the low-level southeasterlies, the environmental winds are light with a speed minimum of 1.5 m s^{-1} at the 500-hPa level. Most of the vertical shear in the sounding is concentrated in the lower levels, resulting in a reverse sheared environment. This type of vertical wind profile is associated with the longevity of convective systems (e.g.,

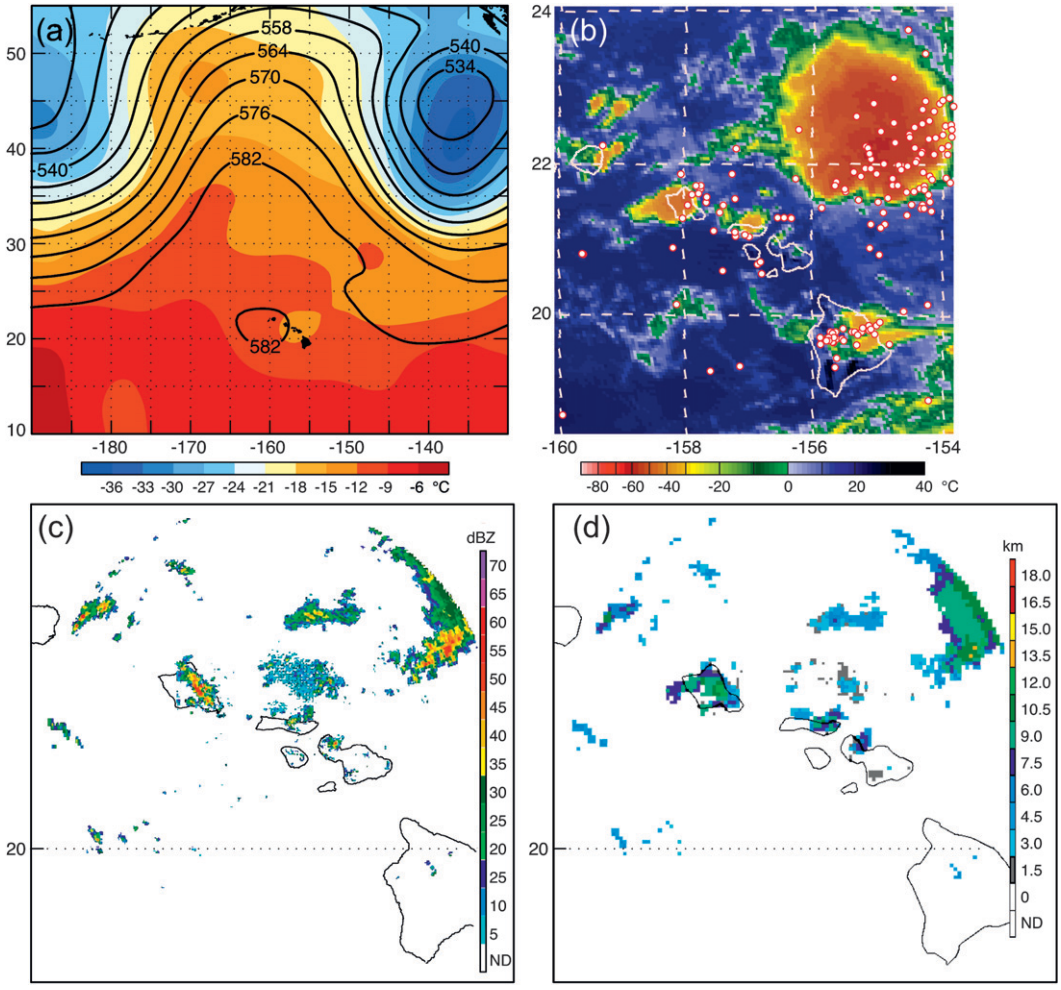

FIG. 4. (a) NCEP–NCAR reanalysis data at 0800 HST 2 Apr 2006 displaying 500-hPa geopotential height contours (decameters) and 500-hPa temperatures (shaded, °C). (b) *GOES-10* infrared image displaying radiative temperature (°C) at 1400 HST 2 Apr 2006 overlaid with PacNet lightning observations (white circles) from 0800 to 1500 HST. (c) Base reflectivity and (d) echo tops from the Molokai radar station at 1320 HST 2 Apr 2006.

Frank 1978; Caracena et al. 1979; Barnes and Sieckman 1984; Rotunno et al. 1988; Nair et al. 1997; Petersen et al. 1999).

c. *Mesoscale analyses*

A large convective system that had formed the previous night can be seen over the ocean to the northeast of Oahu in the 1400 HST infrared satellite imagery (Fig. 4b). This feature stayed stationary throughout most of the day but by the early evening had drifted south, bringing heavy rain to east Maui and the north and east parts of Hawaii Island. Heavy rain on Oahu began midmorning with the Molokai radar detecting echoes indicative of heavy rain over the Koʻolaus from 1000 until almost 1700 HST. Examination of base reflectivity images shows returns of up to more than 50 dBZ along the Koʻolaus during this period (Fig. 4c).

The STP derived from Molokai radar data (Fig. 2c) shows rainfall concentrated along the crest of the Koʻolaus. These data are only available from 1220 to 1740 HST, due to a gap in radar coverage in the late morning. At the lowest elevation scan the bottom of the radar beam is approximately 1 km above sea level near the central Koʻolaus, which is within a few hundred meters of the highest peaks in this region. Comparison of the STP with Oahu rain gauge measurements over the same time interval (Fig. 7) shows that the radar consistently overestimated the accumulated precipitation at the gauges by a factor of approximately 2.

The presence of significant ice particles within the convective clouds that composed the thunderstorm complex is a likely cause of the STP overestimation. Ice particles yield high radar reflectively and can led to overestimations of precipitation (e.g., Fulton 1999); this

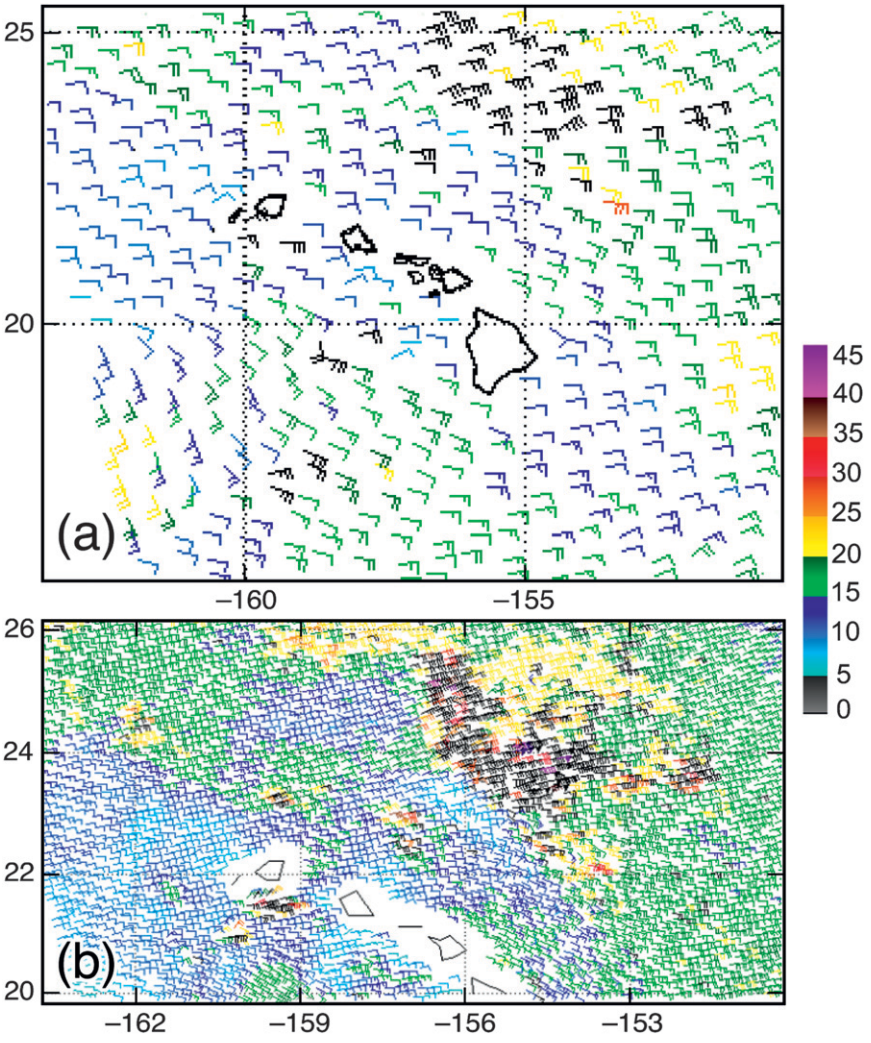

FIG. 5. QuikSCAT satellite-derived near-surface winds (barbs, kt; 1 kt = 0.5144 m s^{-1}) (a) over the Hawaiian Island chain and (b) near Oahu at approximately 0600 HST 2 Apr 2006. Black wind barbs indicate possible rain contamination of the data.

overestimation can be exacerbated as ice particles begin to melt near the freezing level (Austin and Bemis 1950). For these reasons a hail cap, which limits all reflectivity values above a threshold to that threshold, is often applied to reduce any possible overestimation of precipitation (Fulton et al. 1998). The effects of ice particles within the convective clouds would be amplified by the rather high hail cap of 70 dBZ used in the calculation of the STP. Hailstones were not recorded anywhere on Oahu during the event and are rarely found at ground level in the Hawaiian Islands (Takahashi 1987). Despite the differences in the amount of precipitation measured by the two sources, a comparison of Figs. 8a and 2c reveals a close agreement in the general pattern of the precipitation: extreme gradients with maxima over the crest of the Ko‘olaus.

The total accumulated precipitation measured by Oahu rain gauges during the period from 0800 to 1800 HST is shown in Fig. 8b. Rain gauges near the crest of the Ko‘olaus recorded the highest totals with maximum rainfall rates of just over 70 mm h^{-1}. Little precipitation accumulated at gauges near the eastern coast and there was almost no precipitation recorded by gauges in other parts of Oahu. The most intense rainfall gradients occur along the slopes of the Ko‘olaus, particularly near the eastern and southern coastlines. This precipitation pattern contrasts with that observed in the flash flood studied by Schroeder (1977), where the convective system responsible for the flood was anchored to the Ko‘olaus, but the rainfall maxima were found approximately 8 km downstream of the mountain crest.

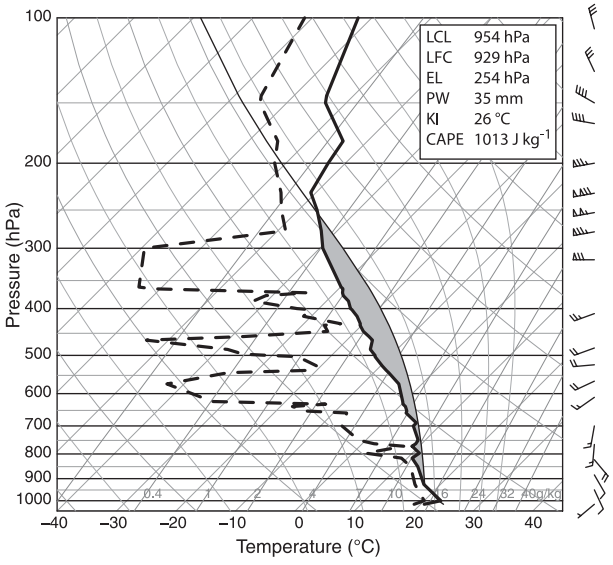

FIG. 6. As in Fig. 3, but from Hilo at 0200 HST 2 Apr 2006.

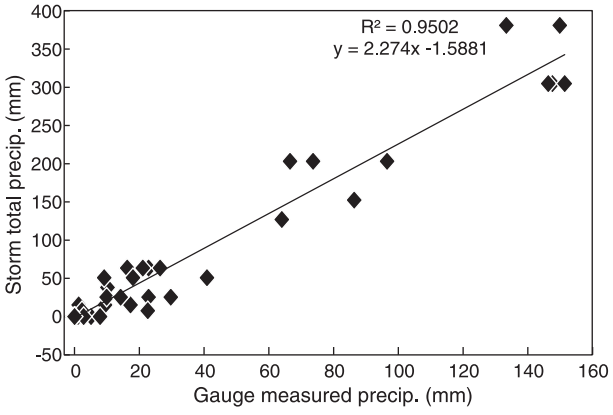

FIG. 7. Scatter diagram of the value of storm total precipitation (mm) from the Molokai radar station at each of the rain gauges locations shown in Fig. 1 vs the accumulated precipitation measured by the corresponding rain gauge from 1220 to 1740 HST. The black line shows a linear least squares fit to the data.

The convection over Oahu was both long lived and deep, extending well above the freezing level. Cloud-top temperatures estimated by infrared sensors on the *GOES-10* satellite during the period of deep convection (Fig. 4b) are just below −40°C over eastern Oahu with a corresponding height of approximately 10 km in the Lihue sounding. The higher spatial resolution of the Molokai radar shows echo tops (Fig. 4d) reaching up to 12 km in the region of the central Ko'olaus, which indicates overshooting cloud tops and intense convection when compared with the equilibrium level of 10.5 km (approximately 250 hPa) calculated from the Lihue sounding. A mean cloud layer wind of 4 m s^{-1} from 77° was computed following the method of Fankhauser (1964) using winds at 850, 700, 500, and 300 hPa from the Lihue sounding (Fig. 3c). This vector was calculated from winds at a station 130 km away from the thunderstorm itself and does not represent actual cloud motion; however, the speed component of the vector is clearly small and reflects the weak environmental winds throughout most of the cloud layer.

Weather observers stationed at HNL and HNG reported cumulonimbus clouds and both intracloud (IC) and cloud-to-ground (CG) lightning strikes over the Ko'olaus from approximately 1000 until 1600 HST. During this period, lightning frequency was reported as occasional (less than 1 flash per minute) except between 1030 and 1100 HST when the HNG station reported frequent (1–6 flashes per minute). The Pacific Lightning

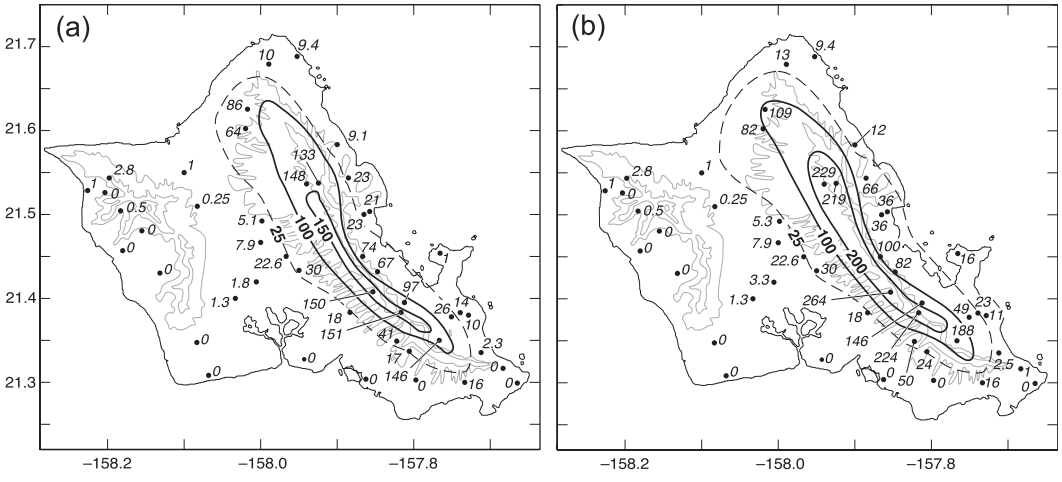

FIG. 8. Total accumulated precipitation (mm) measured by Oahu rain gauges from (a) 1220 to 1740 and (b) 0800 to 1800 HST 2 Apr 2006.

Detection Network (PacNet) recorded 11 CG lightning strikes over Oahu from 0800 until 1500 HST (Fig. 4b). The low strike count from PacNet is likely due to the network's inability to detect IC lightning strikes and its detection efficiency for CG strikes of approximately 50% (Pessi et al. 2009). These observations and remote sensing of lightning indicate that the Oahu thunderstorm complex had significant electrical activity for most of its duration. The presence of lightning suggests that the thunderstorm complex contained a substantial amount of graupel particles above the freezing level (e.g., Saunders 1993), which provides indirect evidence that the overestimation of rainfall by the Molokai radar derived STP was caused by ice particles.

Surface-observing stations recorded wind speeds increasing over Oahu during the late morning and early afternoon. Wind directions around the island vary greatly with a shift toward an onshore component midday, indicative of a sea-breeze circulation pattern. The HNG station recorded relative humidity above 80% throughout the day (Fig. 9a). The measurements from this station, which is located upstream of the central Koʻolaus (Fig. 1), indicate the high moisture content of the low-level flow incident on eastern Oahu. HNG also recorded a dramatic wind shift (Fig. 9b) with calm winds throughout the night and early morning until 1000 HST after which 5 m s^{-1} easterlies with higher gusts were recorded. This wind shift coincides with the accumulation of the majority of the precipitation recorded at HNG (Fig. 9c) and the first observations of cumulonimbus clouds and lightning.

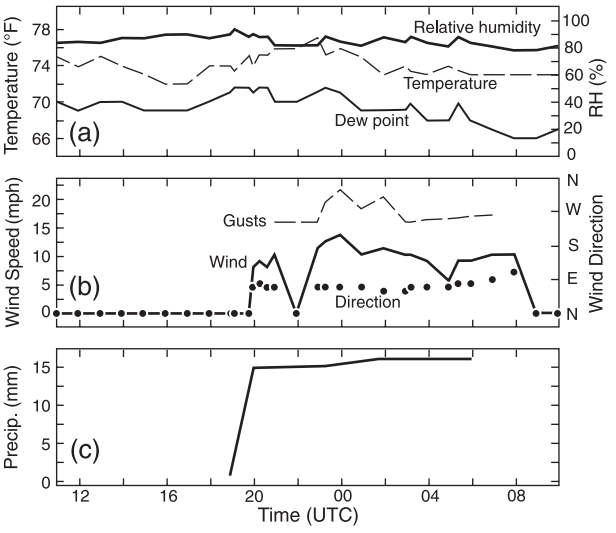

FIG. 9. The HNG station observations from 0000 to 2400 HST 2 Apr 2006: (a) RH, T, and T_d; (b) wind; and (c) precipitation.

3. Model configuration

The WRF model is a state-of-the-art mesoscale numerical modeling system designed for both research and operational applications. The equation set is fully compressible, Euler nonhydrostatic, and has a terrain-following, hydrostatic pressure vertical coordinate. This study employs version 3.0.1 of the Advanced Research WRF (ARW-WRF) dynamical core in the simulation of the 2 April 2006 flash-flooding event on Oahu. A detailed description of the ARW-WRF can be found in Skamarock et al. (2008).

The application of the mesoscale model to a particular area of interest is made by configuring a system of nested grids, the design of which is strongly influenced by the data available for definition of the model's initial and boundary conditions. Over the Hawaiian Islands and their adjacent waters the highest resolution data available are from the National Centers for Environmental Prediction's (NCEP) final operational global analysis (FNL), which is available 6-hourly on a global 1° × 1° grid with 26 pressure levels. Initial and boundary conditions for the model are provided by the FNL dataset with the following exceptions: land surface data were defined by the NCEP North American Regional Reanalysis (NARR) at 32-km horizontal resolution; typical values of soil moisture for a Hawaiian forest (Giambelluca et al. 2009) were inserted into these data; sea surface temperature (SST) is defined by the NCEP real-time SST analyses at 0.5° global resolution.

This combination of atmospheric and land surface data is fed into a system of five computational grids connected by two-way interacting nests (Fig. 10). The telescoping structure of the nests culminates in a high-resolution grid over Oahu. The WRF model's multiple two-way nesting feature is essential to this study as it allows detailed representation of the atmosphere's interaction with the complex topography of the islands, while at the same time modeling the synoptic-scale features. The horizontal resolutions of each of the grids from outermost (D1) to innermost (D5) are, respectively, 40.5 km, 13.5 km, 4.5 km, 1.5 km, and 500 m, with corresponding mesh sizes of 109 × 84, 108 × 81, 183 × 123, 270 × 144, and 180 × 165 points. The time steps for each grid from D1 to D5 are 180, 60, 20, 6.7, and 2.2 s. Each grid contains 40 computational layers with the highest vertical resolution in the lowest 2 km and the lowest atmospheric layer at approximately 30 m above ground level.

Surface terrain features of the Hawaiian Islands are defined using two data sources. The general terrestrial input files supply albedo, greenness fraction, slope category, and deep soil temperature at a resolution of 1°. USGS terrestrial data with a resolution of 30 s (approximately 1 km) supply topography, land use, and soil

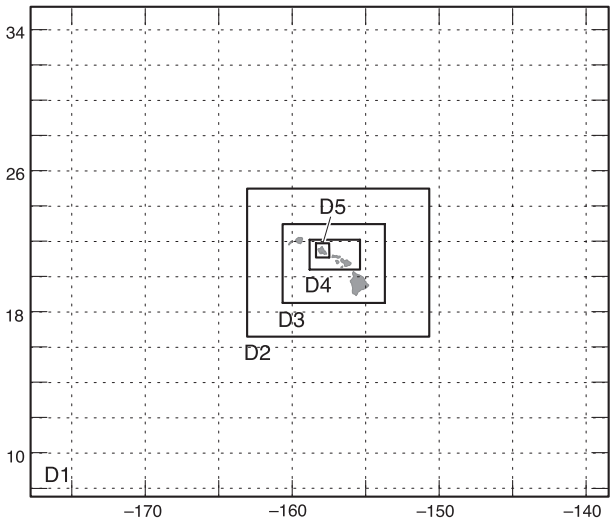

FIG. 10. The system of nested grids used in the simulation with the coarse outer grid (D1) taking up the entire map. The high-resolution innermost grid (D5) forms a box over Oahu.

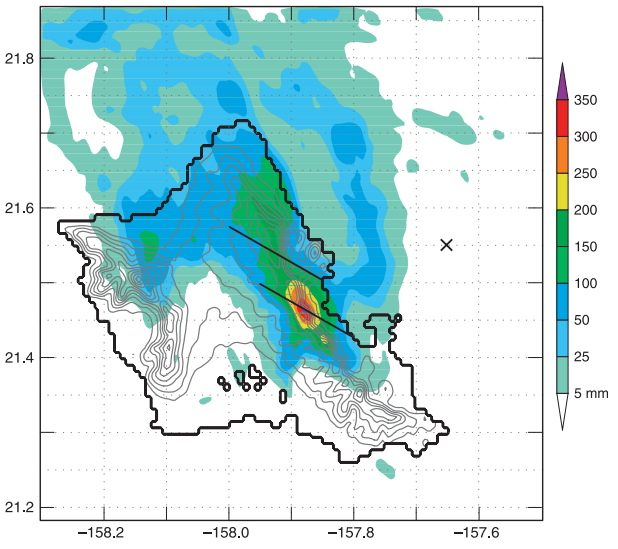

FIG. 11. Simulated accumulated precipitation (mm, shaded) on the innermost grid (D5) from 0800 to 1800 HST 2 Apr 2006. Model terrain height contours are plotted in 100-m increments. The black lines mark the locations of the cross sections shown in Fig. 17 and the black X marks the location of the sounding shown in Fig. 12.

type. The model orography on the innermost grid (D5) is shown in Fig. 11. Although this grid has a 500-m horizontal resolution, the terrain data are smoothed to 1-km resolution, resulting in shallower valleys, lower ridges, and the complete omission of many small-scale orographic features.

The following physical parameterizations were used in the simulation. For the planetary boundary layer, the Yonsei University scheme based on Hong et al. (2006) is employed along with the accompanying surface layer scheme. We use a parameterization of shortwave radiation based on Dudhia (1989) and the Rapid Radiative Transfer Model (Mlawer et al. 1997) to parameterize the longwave radiation. Microphysics are parameterized using the Purdue–Lin scheme (Lin et al. 1983; Chen and Sun 2002), which includes mixed-phase processes and six classes of hydrometeors. Also employed was the Noah land surface model (LSM; see Ek et al. 2003). This LSM has soil temperature and moisture on four layers along with vegetative effects and an urban canopy model.

The Betts–Miller–Janjic scheme (Betts and Miller 1986; Janjic 1994) is used to parameterize cumulus convection in the outermost two domains with all other domains using a detailed treatment of cloud with bulk microphysics. Studies have shown (Warner and Hsu 2000; Wapler et al. 2010) that the convection resolved on the inner grids of a nested system is sensitive to the cumulus parameterization employed on the outer grids. Sensitivity tests run using the Kain–Fritsch parameterization (Kain and Fritsch 1993) in the outer two domains resulted in significantly less precipitation (approximately 50 mm lower than observations in many areas) than the Betts–Miller–Janjic parameterization. This result agrees with the study by Warner and Hsu (2000), which found that use of the Kain–Fritsch parameterization scheme led to the underestimation of the inner-grid precipitation more than any other scheme.

Use of the relatively coarse FNL data requires a period of time for the model to ingest the data, to "spin up" the microphysical variables, and to become stable at the convective scale. This spinup period can have indirect impacts long after model initialization; particularly in higher-resolution simulations (see Clark et al. 2007). The simulation was run for a total of 36 h with model initiation at 1400 HST 1 April 2006, allowing approximately 12 h before the time of any observed convection near Oahu for the simulation to become stable. Sensitivity tests run with shorter spinup periods were much less successful in simulating the observed pattern of precipitation.

4. Model results

A vertical profile was taken inside the highest-resolution grid at 0800 HST (Fig. 12) with the location of the profile marked in Fig. 11. This simulated sounding displays a moist environment below 450 hPa. A reverse sheared wind profile is simulated with weak midlevel winds above moderate southeasterly flow at low levels. The inverted trough at the surface is also represented with the direction of the simulated low-level winds (Fig. 13) in good agreement with observations from the

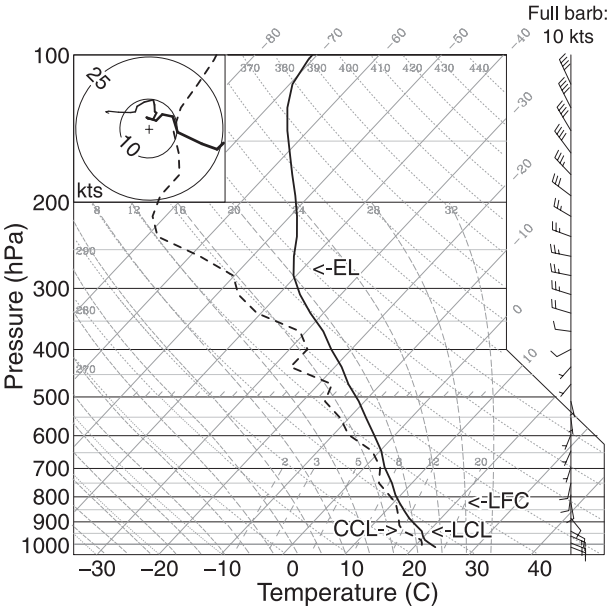

FIG. 12. Simulated skew T–log$p$ diagram from offshore of Oahu's windward coast (location marked in Fig. 11) at 0800 HST 2 Apr 2006. Wind barbs are standard convention. LCL, convective condensation level (CCL), LFC, and EL are indicated.

morning scatterometer pass (Fig. 5). The vertical wind profile in Fig. 12 closely matches that in the Lihue sounding (Fig. 3c) except in the 250–350-hPa layer where the wind directions differ by 180°. Satellite imagery shows the anvil of the thunderstorm complex extending west of the Ko'olaus (Fig. 4b), indicating easterly winds near cloud top, which corresponds to the easterly winds near the equilibrium level in the Lihue sounding. In general, the simulated synoptic-scale environment over the Hawaiian Islands provides an accurate representation of the synoptic conditions on 2 April 2006 with the notable exception of the upper-level westerlies penetrating lower into the atmosphere than observations indicate.

a. Mesoscale

The simulated pattern of precipitation on Oahu (Fig. 11) is closely linked with the orography. The WRF model successfully simulated a pattern of precipitation indicative of terrain anchoring of convection with extreme gradients of rainfall near the eastern coast and the highest precipitation totals over the crest of the Ko'olaus. A direct comparison was made of the simulated precipitation to the corresponding rain gauge observations with the gauges divided into three groups by their location with respect to the orography (Fig. 14). The gauges within each group are listed from northernmost to southernmost along the abscissa of Fig. 14.

Between the Ko'olaus and the northeast coastline (Fig. 14i), the simulated precipitation is overestimated at northern gauges and underestimated at southern gauges. Over the Ko'olaus (Fig. 14ii) accumulated precipitation was slightly underestimated by the model at gauges in the northern part of the range, overestimated at gauges in the central part of the range, and significantly

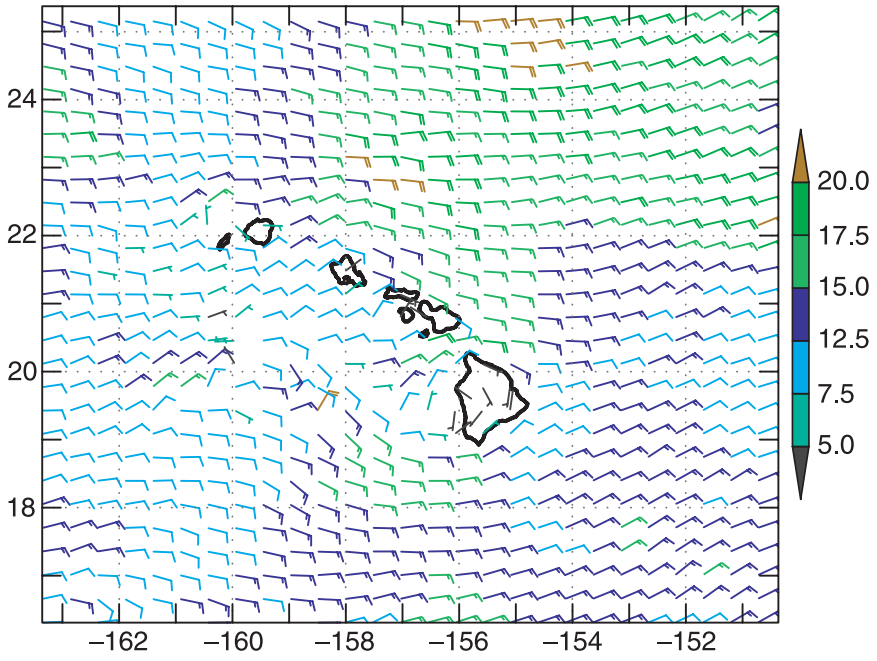

FIG. 13. Simulated 10-m winds (kt) at 0600 HST 2 Apr 2006.

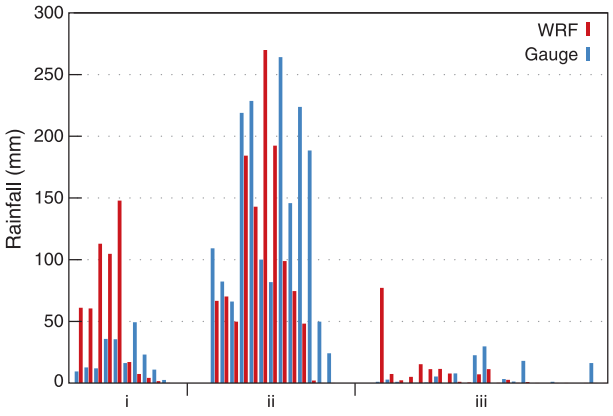

FIG. 14. Accumulated rainfall (mm) from 0800 to 1800 HST 2 Apr 2006 measured by Oahu rain gauges (blue) and simulated by WRF at the corresponding gauge location (red). The gauges have been grouped by location into those (i) east, (ii) along, and (iii) west of the Koʻolau Mountain Range. Within each group the gauges are listed with the northernmost (southernmost) on the left-hand (right hand) side.

underestimated in the southern part of the range. West of the Koʻolaus (Fig. 14iii), the simulation produces little precipitation, in good agreement with observations, except in the far north near the Waianae Mountains. Despite substantial disagreement with observations at many individual gauges, the WRF model was able to successfully simulate the general pattern of observed precipitation in each of the three groups shown in Fig. 14 with the exception of southeastern Oahu where precipitation was significantly underestimated.

Along the northern Koʻolaus, the simulation generates maximum rainfall rates of just over 60 mm h^{-1}. The observed rainfall rate at the two rain gauges closest to the crest of the northern Koʻolaus (see Fig. 1) was approximately 65 mm h^{-1} during the period of heavy rain. The maximum simulated rainfall rate at the location of the simulated rainfall maximum in the central Koʻolaus is approximately 100 mm h^{-1}, which is higher than anything recorded by rain gauges near that area but is not unprecedented in Hawaiian heavy rain events (e.g., Fullerton and Wilson 1975).

The simulated low-level wind field (Fig. 15) is strongly influenced by the topography and thermal circulation patterns (Leopold 1949). In the early morning, winds over Oahu are light and generally blowing offshore (Fig. 15a). A zone of confluence of the low-level wind can be seen off the coast to the east of the Koʻolaus where offshore flow meets the easterlies over the open ocean. By 0800 HST in the simulation, convection formed in this offshore confluent zone and became vigorous. Significant rainfall accumulates offshore by 1100 HST (Fig. 11). Simulated rainfall then dissipates offshore and begins accumulating on the Koʻolaus by just after 1100 HST lasting until approximately 1700 HST. Vigorous deep convection and heavy rainfall remains fixed over the northern and central Koʻolaus for approximately 5 h during this period. Convection also forms over the northern slopes of the Waianae Mountains in the afternoon.

By the afternoon, the winds have an onshore component with the easterlies increasing and flowing over the Koʻolaus (Fig. 15b). Easterly winds near the surface flow into the eastern Koʻolaus for the duration of the simulated convection over the Koʻolaus. Simulated local wind maxima of over 13 m s^{-1} are present north and south of Maui and Molokai with light winds to the lee of all the islands (Fig. 15c). The wind pattern in the simulation agrees well with station observations at HNG (Fig. 9b). Observations from HNL, however, show much less of an onshore wind component in the afternoon than the simulation generates.

To investigate the role of the orography on the simulated thunderstorm complex, time averages of the level of free convection (LFC) and vertical velocity were made on grid D5. These time averages were made during the period of deep convection over the Koʻolaus, between 1100 and 1700 HST, using model output with a temporal frequency of 20 min. The LFC along the eastern slopes of the central Koʻolaus ranges from 600- to 300-m altitude (Fig. 16a) with higher values over the slopes of the northern Koʻolaus. These LFCs are somewhat lower than the 985 m calculated from the Lihue sounding; however, weather observers at the HNG station reported cumulonimbus clouds with bases at approximately 450-m altitude over the central Koʻolaus throughout the period of 0900–1700 HST. The lifting condensation level (LCL), which provides a reasonable approximation of cloud-base height (e.g., Craven et al. 2002), is slightly lower than the LFC in both the simulated (Fig. 12) and observed (Fig. 3c) environmental profiles. This suggests that simulated cloud bases in the central Koʻolaus are near or slightly below observations.

The time-averaged vertical velocity field on the 900-hPa surface (Fig. 16b) shows persistent regions of upward vertical motion over the steep eastern slopes of the Koʻolaus. The Koʻolau Mountains lift the moist low-level flow above its LFC, initiating moist ascent in the simulation. The averaged vertical velocity is strong high into the troposphere with the greatest velocities at the 500-hPa level directly over the central Koʻolaus (Fig. 16c). The vertical shear vectors calculated from the winds at the 900- and 500-hPa levels are 7.7 m s^{-1} at 110° from the Lihue sounding (Fig. 3c) and 3.1 m s^{-1} at 110° from the simulated sounding (Fig. 12). Close examination of Fig. 16 reveals a downshear (northwest) tilt

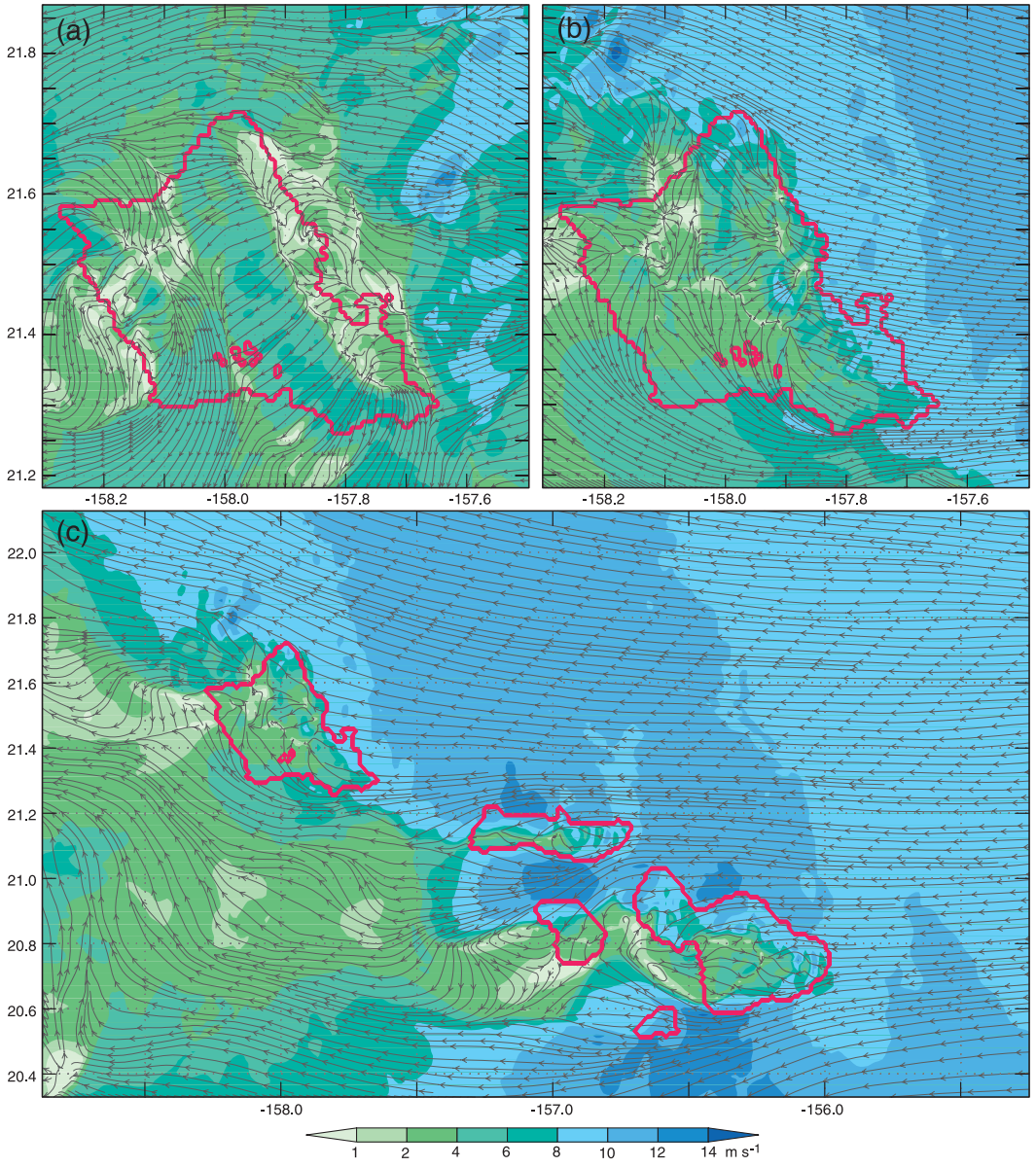

FIG. 15. Simulated horizontal wind speed (shaded, m s^{-1}) and streamlines on the lowest model level plotted on (a) grid D5 at 0500 HST, (b) grid D5 at 1400 HST, and (c) grid D4 at 1400 HST on 2 Apr 2006.

of the vertical velocity field over the Ko‘olaus between the 900- and 500-hPa levels, particularly over the northern Ko‘olaus.

b. Microphysics

To show the structure of the simulated convective cells, two transects were taken along lines (indicated in Fig. 11) roughly parallel to the mean direction of the environmental winds in the lowest 3 km. These vertical cross sections are representative of mature convective cells of the simulated thunderstorm complex in the northern (Figs. 17a and 17c) and central Ko‘olaus (Figs. 17b and 17d). The vertical velocity fields (Figs. 17a and 17b) show a strong updraft with a pronounced northwestward tilting with height throughout the lower levels. The orientation of this vertical tilt is aligned downshear of the low-level environmental flow; a feature commonly seen in updrafts that form in a vertically sheared environment (e.g., Weisman and Klemp 1984). This sloping of the simulated updrafts in low levels is characteristic of long-lived convective systems (e.g., Rotunno et al. 1988).

The rainwater mixing-ratio fields (Figs. 17a and 17b) show rain falling downshear of the updraft where

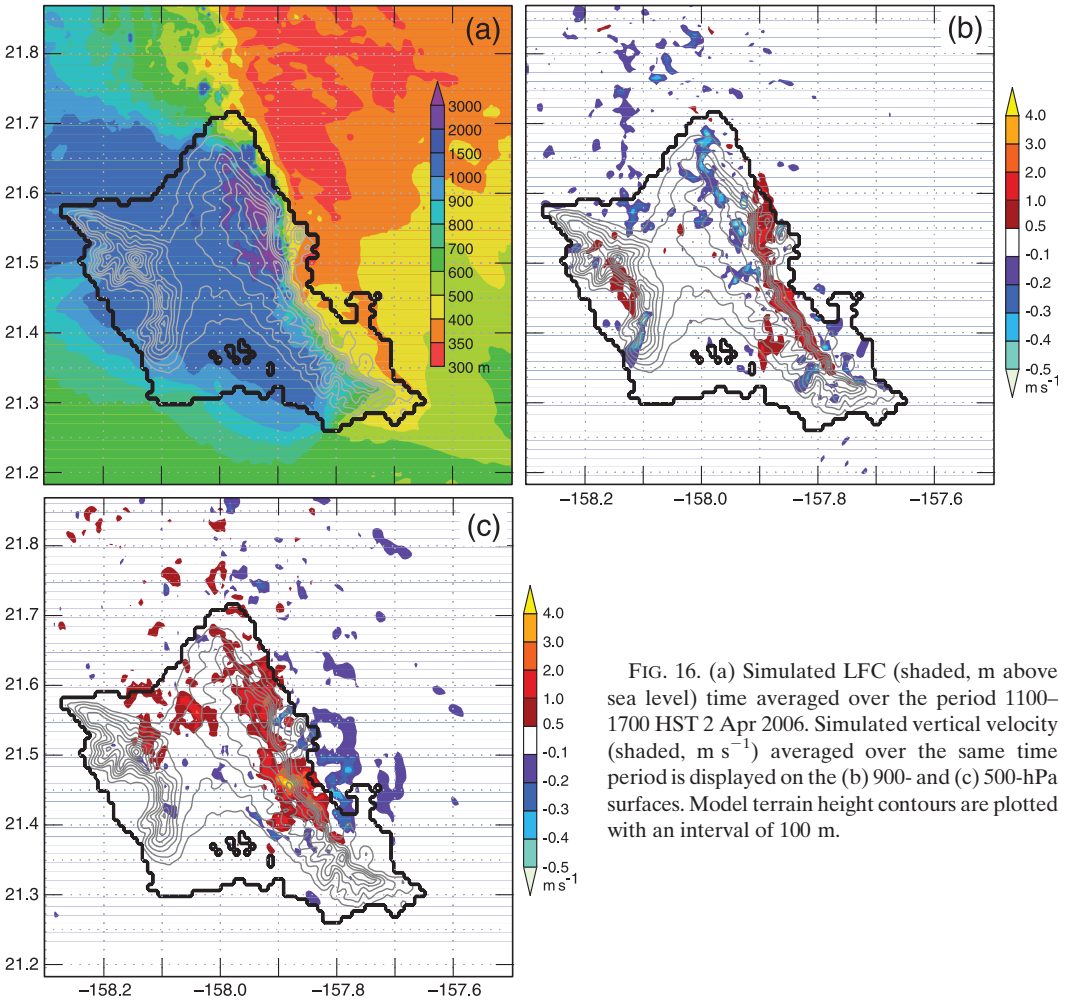

FIG. 16. (a) Simulated LFC (shaded, m above sea level) time averaged over the period 1100–1700 HST 2 Apr 2006. Simulated vertical velocity (shaded, m s^{-1}) averaged over the same time period is displayed on the (b) 900- and (c) 500-hPa surfaces. Model terrain height contours are plotted with an interval of 100 m.

moderate convective downdrafts are also present. The tilted structure of the updraft enables raindrops to fall out of its lower parts. This unloads liquid water from the updraft and separates the main rainshaft and downdrafts from the inflow of moist air, helping to sustain the convection (Ludlam 1963). The southeast-to-northwest orientation of the Ko'olaus combined with the northwestward sloping of the updrafts results in rain falling out of the updraft and onto the crest of the mountain range. The weak environmental flow at midlevels in the simulation (Fig. 12) minimizes the horizontal tracking of cells, facilitating a quasi-stationary thunderstorm complex over the Ko'olaus.

The simulated convective cell from the central Ko'olaus (Figs. 17b and 17d) formed over the center of the simulated rainfall maximum (Fig. 11). Accumulated rainfall at this grid point was higher than nearby rain gauge measurements, suggesting this convective cell is more intense than representative cells of the observed thunderstorm complex. The graupel mixing ratio (Fig. 17b) reaches a maximum of just over 9 g kg^{-1} (approximately 4.6 g m^{-3}) and coincides with the strongest vertical velocities of just over 20 m s^{-1}. The high concentration of graupel results in the 50-dBZ simulated radar reflectivity contour reaching up to nearly 8 km (Fig. 17d), which corresponds closely to radar cross sections of an intense convective cell that formed over eastern Maui (Lyman et al. 2005). This mass of graupel is somewhat higher than values seen in simulations of vigorous convective clouds in Texas performed by Khain et al. (2004). Few observations of hydrometeor contents within cumulonimbus clouds exist that could be used for comparison with these model results; however, observations of cumulus congestus clouds in northeastern Colorado have shown moist-adiabatic cores within the updrafts (Heymsfield et al. 1978). The simulated total hydrometeor water content in the location of the graupel maximum is approximately 4.8 g m^{-3}. Advection of graupel from lower levels may help account for the large hydrometeor water content in the upper portion of

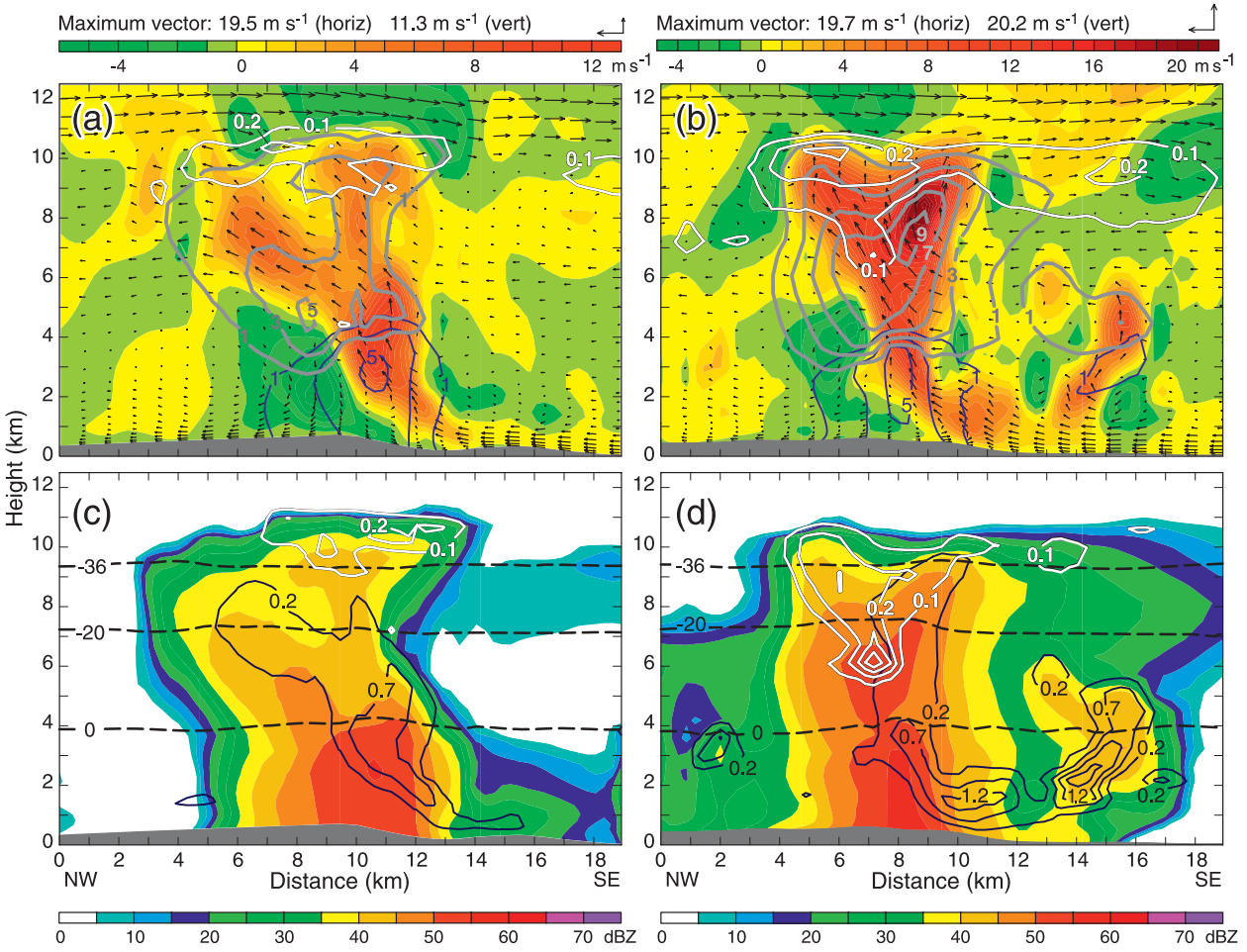

FIG. 17. Vertical cross sections of simulated convection over the Ko'olaus with horizontal orientation shown by the (a),(c) northernmost and (b),(d) southernmost transects in Fig. 11. These cross section were taken at (a),(c) 1540 and (b),(d) 1400 HST and display (a),(b) simulated vertical velocity (shaded, cm s^{-1}), rainwater mixing ratio (blue contours, g kg^{-1}), graupel mixing ratio (gray contours, g kg^{-1}), snow mixing ratio (white contours, g kg^{-1}), and circulation vectors and (c),(d) simulated radar reflectivity (shaded, dBZ), isotherms (dashed contours, °C), cloud liquid water mixing ratio (dark blue contours, g kg^{-1}), and cloud ice mixing ratio (white contours, g kg^{-1}).

the updraft. Regardless, this value is well below the adiabatic liquid water content of almost 6 g m^{-3}, calculated using the cloud-base temperature (15°C) and height (900 hPa) from the Lihue sounding (Browning 1963).

While the simulated cell from the northern Ko'olaus (Figs. 17a and 17c) is probably more representative of the observed thunderstorm complex, both of the cells shown in Fig. 17 conform to the available observations. Simulated radar reflectivity (Figs. 17c and 17d) displays echo tops of 10–11 km, which is in close agreement with echo-top heights measured by the Molokai radar (Fig. 4d). Although full-volume radar data are not available for a more direct observation, a substantial amount of frozen precipitation particles is the most likely cause for the overestimation of storm total precipitation by the Molokai radar. In agreement with this observation the simulated convective cells contain a large mass of graupel and high reflectivity values above the 0°C isotherm. Both of the simulated cells shown in Fig. 17 contain simulated ice particles, supercooled water droplets, and graupel above the 0°C isotherm. The presence of these microphysical specimens is associated with charge separation and lightning (e.g., Saunders 1993), consistent with observations of lightning throughout the duration of the thunderstorm complex. Cloud liquid water content levels in the simulated mixed-phase region (between the 0° and 20°C isotherms) are within values conducive to the negative charging of graupel particles, according to laboratory experiments (Takahashi 1978; Saunders et al. 1991; Pereyra et al. 2000).

The time variation of the vertical distribution of various hydrometeors generated by the model is shown in Fig. 18. Rather than displaying the hydrometeor concentration

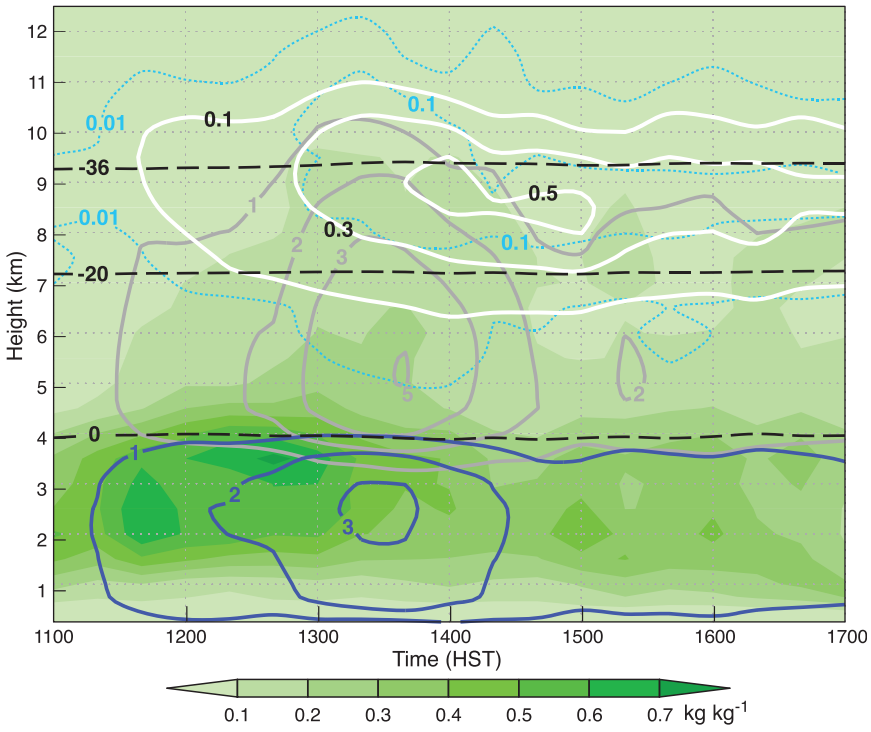

FIG. 18. Time–height cross section of rainwater mixing ratio (blue contours, kg kg^{-1}), graupel mixing ratio (gray contours, kg kg^{-1}), snow mixing ratio (solid white contours, kg kg^{-1}), cloud liquid water mixing ratio (shaded, kg kg^{-1}), cloud ice mixing ratio (dotted light blue contours, kg kg^{-1}), and isotherms (dashed contours, °C). The values for each hydrometeor are summations over a rectangle encompassing the Ko'olau Mountain Range (21.3°–21.7°N and 158.05°–157.7°W). Horizontal axis is time (HST) and vertical axis is height (km).

at a specific location, the horizontal summation of each hydrometeor type within a rectangular area (21.3°–21.7°N and 158.05°–157.7°W) over the Ko'olaus is displayed. The portion of a cloud between the 0°C isotherm and the cloud base is known as the coalescence zone and the convective cells at both of the locations shown in Fig. 17 as well as in Fig. 18 have coalescence zones of more than 3 km in depth. Throughout these deep coalescence zones, large amounts of rain and cloud liquid water (Figs. 17 and 18) are present, indicating that the condensation and collision and coalescence of droplets is taking place in this region.

Raindrops are the first precipitation-size hydrometeor simulated over the Ko'olaus in large concentrations, followed by graupel and then snow (Fig. 18). The percentage of graupel embryos formed by raindrop freezing has been observed to increase with increasing cloud-base temperature (Knight 1981). The low cloud bases in the observed and simulated convective cells along with the sequence of hydrometeor formation displayed in Fig. 18 indicate that the majority of the graupel originated from the freezing of raindrops formed in the coalescence zone as they were advected within the updraft (e.g., Phillips et al. 2001). Evidence for the initial formation of hailstones by the freezing of raindrops was found by Takahashi (1987) in his study of hailstones collected at ground level during a thunderstorm over Hawaii Island.

As the simulated thunderstorm complex evolved, the mass of cloud water droplets and graupel particles in the mixed-phase region increased (Fig. 18) with maxima at approximately 1330 HST. This environment was favorable for the growth of graupel particles by riming with supercooled cloud droplets (Pflaum and Pruppacher 1979), with the eventual melting of these ice particles contributing substantially to the production of rainfall. The formation and growth of graupel was facilitated by a strong vertical flux of condensate above the 0°C isotherm during the early and middle stages of the thunderstorm complex. The maximum concentration of snow over the Ko'olaus at any given time is nearly an order of magnitude less than that of graupel or rain, indicating that the riming of snow to form graupel contributed little to the total mass of graupel. An environment conducive to charge separation, with ice particles, graupel, and supercooled water coexisting in the mixed-phase region, is present

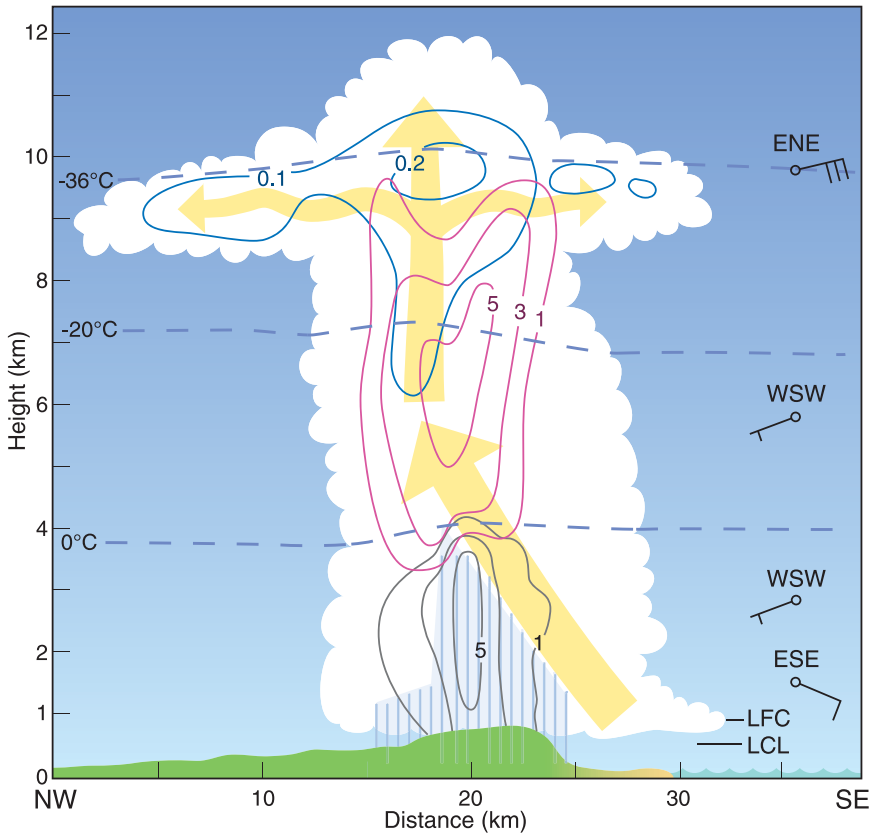

FIG. 19. Conceptual model of a mature convective cell of the 2 Apr 2006 thunderstorm complex. This schematic diagram displays a southeast-to-northwest cross section taken through the central Koʻolaus. LCL, LFC, environmental winds, and temperatures are from the Lihue sounding. Rain water mixing ratio (gray contours, g kg^{-1}), graupel mixing ratio (pink contours, g kg^{-1}), snow mixing ratio (blue contours, g kg^{-1}), and cloud circulations (bold arrows) are from the mesoscale model output.

throughout the mature phase of the simulated thunderstorm complex (Fig. 18).

5. Conclusions and discussion

a. Summary and conclusions

This study examines a thunderstorm complex that remained nearly stationary over the Koʻolau Mountain Range for more than 6 h on 2 April 2006. The event was one of three cases of heavy rainfall focused on the Koʻolaus that occurred during an unusually wet period in the spring of 2006. Each of these events produced flash flooding in many of the low-capacity northeast-facing watersheds of eastern Oahu. These storms formed under the influence of a recurring midlevel trough in an environment with low-level southeast flow, moderate conditional instability, enhanced midlevel moisture content, and westerly shear of the environmental winds with height in the lower levels.

A case study of the 2 April event was undertaken to better understand the interaction of moist southeast flow with the complex terrain of Oahu. High-resolution numerical simulations of this event employing the ARW-WRF mesoscale model successfully generated a pattern of precipitation indicative of convection anchored by the orography of the Koʻolaus. The characteristics of the simulated convection were investigated and compared with observations made during the event.

The results of the simulations were combined with observations to produce a schematic diagram of the thunderstorm complex (Fig. 19). The convection over Oahu was sustained by a steady flux of moist conditionally unstable air into the Koʻolaus by the easterly flow at the surface. Lifting by the eastern slopes of the Koʻolaus created the ascent needed for the moist low-level air to reach its level of free convection, triggering vigorous convective development and the repeat formation of convective cells. Westerly shear of the low-level flow was crucial in organizing the convection. The

turning of the environmental winds from easterly near the surface to southeasterly near and above the mountaintop, combined with light winds at midlevels, resulted in convective updrafts that tilted northwestward with height throughout the lowest 3 km. Weak midlevel winds over the strong low-level shear anchored the lower portion of the convection to the mountains, resulting in minimal horizontal cloud motion and a quasi-stationary convective system. The slope of the updrafts had a large component parallel to the axis of the mountain range, which resulted in the main rainshaft of the convective cells extending along the crest of the Koʻolaus. In addition to determining the pattern of accumulated precipitation, this tilted updraft structure contributed to the longevity of the thunderstorm complex by keeping rainfall and downdrafts separate from the inflow of warm moist air.

The formation of rainfall was complex and involved mixed-phase microphysical processes. The vertical advection of condensate originating below the freezing level by vigorous convective updrafts was crucial in the formation and growth of graupel. These graupel particles formed through the freezing of raindrops and grew by riming with supercooled cloud droplets. This process resulted in a substantial amount of frozen precipitation particles and created an environment conducive to charge separation and lightning in the mixed-phase region.

b. Discussion and speculation

The pattern of accumulated precipitation in each of the spring 2006 heavy rain events exhibited extreme gradients with maxima on the crest of the Koʻolaus, a pattern characteristic of Oahu flooding events that occur under southeast low-level flow (see Fig. 2). This pattern of accumulated precipitation differs from patterns found in other studies of Oahu heavy rain events (e.g., Schroeder 1977; Dracup et al. 1991). While all three spring 2006 events share easterly flow at the surface and southeasterly environmental flow from just above the surface to approximately the 750-hPa level, the static stability exhibited by the atmospheric profiles differs significantly (Fig. 3). The 2 April event had the most unstable vertical profile and deep convective development (Fig. 3c), while the 1 March event had much less instability and relatively shallow convection (Fig. 3a). We suggest that the differences in the pattern of precipitation between these two events (Figs. 2a and 2c) are due in part to the depths of the convection in each case. In contrast to the quasi-stationary thunderstorm complex observed in the 2 April event, shallow convection with cloud tops near 700 hPa would tend to be advected northwestward along the axis of the Koʻolaus Mountain Range by the southeasterly mean cloud layer winds. This northwest tracking of convective cells could explain the precipitation maximum in the northern part of the mountain range seen in the 1 March event. The vertical wind profiles in these two events are similar, but the thermodynamic instability and depth of the resulting convection differ substantially and result in different cloud dynamics and associated patterns of precipitation.

Studies of cloud electrification in both the tropics and midlatitudes have found low cloud bases, deep coalescence zones, and high precipitation yields to be associated with decreased lightning flash rates (Williams et al. 1992; Rutledge et al. 1992; Williams et al. 2005). This reduction in lightning results from the formation of rainfall and the removal of condensate from the updraft in the coalescence zone, thereby robbing the mixed-phase region of cloud water (Williams et al. 2005). Nevertheless, in the simulation presented in this study, vertical advection of hydrometeors that formed within a deep and active coalescence zone led to an environment conducive to charge separation. The combination of an active precipitation process below the freezing level and exceptionally long-lived and nearly stationary vertical motion over the Koʻolaus enabled the modest lightning flash rates observed in the thunderstorm complex.

Simulated convective cells repeatedly formed over the crescent-shaped region of the Koʻolaus to the west of the HNG station. The geometry of the Koʻolaus in this area appears to have played an important role in focusing and lifting the low-level flow and initiating convective cells nearby. Lin et al. (2001) studied numerous orographic heavy rain events in various parts of the world and found that convection often began in a horizontally concave region of the mountain range, as was the case in this study. The results of the Oahu simulations suggest that the enhanced convergence of moisture in this concave region of the Koʻolaus lowered the level of free convection (Fig. 16a), resulting in more vigorous buoyant ascent of these air parcels when lifted by the orography.

Future research on anchoring of convection to the Koʻolau Mountain Range under southeast flow should include detailed analyses of full radar volume data from multiple events, if and when these data become available. Idealized mesoscale simulations using environmental profiles with various combinations of vertical wind shear and thermodynamic instability could be useful in confirming the role of Oahu's orography in focusing areas of heavy rain under conditions of southeast low-level flow.

Acknowledgments. The authors benefited greatly from discussions with Drs. Vaughan Phillips, Thomas Schroeder, and Christopher Chambers. This manuscript

was substantially improved by the thorough reviews of two anonymous reviewers. Tiziana Cherubini and Antti Pessi provided technical support, Kevin Kodama and Ryan Lyman supplied observational data, and Nancy Hulbirt provided her graphical expertise. Computational resources were provided by NCAR's Bluefire and MHPCC's Hurricane machines. This work was supported by the Office of Naval Research under Grants N000140510551 and N000140810450.

REFERENCES

Akaeda, K., J. Reisner, and D. Parsons, 1995: The role of mesoscale and topographically induced circulations in initiating a flash flood observed during the TAMEX project. *Mon. Wea. Rev.,* **123,** 1720–1739.

Austin, P. M., and A. C. Bemis, 1950: A quantitative study of the brightband in radar precipitation echoes. *J. Meteor.,* **7,** 145–151.

Barnes, G. M., and K. Sieckman, 1984: The environment of fast- and slow-moving tropical mesoscale convective cloud lines. *Mon. Wea. Rev.,* **112,** 1782–1794.

Betts, A. K., and M. J. Miller, 1986: A new convective adjustment scheme. Part II: Single column tests using GATE wave, BOMEX, and arctic air-mass data sets. *Quart. J. Roy. Meteor. Soc.,* **112,** 693–709.

Blumenstock, D. L., and S. Price, 1967: Climates of the United States—Hawaii. Climatography of the United States 60-51, ESSA, 27 pp. [Available from NOAA Central Library, 2nd Fl., SSMC3, 1315 East–West Highway, Silver Spring, MD 20910.]

Browning, K. A., 1963: The growth environment of hailstones. *Meteor. Mag.,* **96,** 202–211.

Caracena, F., R. A. Maddox, L. R. Hoxit, and C. F. Chappell, 1979: Mesoanalysis of the Big Thompson storm. *Mon. Wea. Rev.,* **107,** 1–17.

Chen, S.-H., and W.-Y. Sun, 2002: A one-dimensional time dependent cloud model. *J. Meteor. Soc. Japan,* **80,** 99–118.

Clark, A. J., W. A. Gallus Jr., and T.-C. Chen, 2007: Comparison of the diurnal cycle in convection-resolving and non-convection-resolving mesoscale models. *Mon. Wea. Rev.,* **135,** 3456–3473.

Cram, R. S., and H. R. Tatum, 1979: Record torrential rainstorms on the island of Hawaii, January–February 1979. *Mon. Wea. Rev.,* **107,** 1653–1662.

Craven, J. P., R. E. Jewell, and H. E. Brooks, 2002: Comparison between observed convective cloud-base heights and lifting condensation level for two different lifted parcels. *Wea. Forecasting,* **17,** 885–890.

Dracup, J. A., E. D. H. Cheng, J. M. Nigg, and T. A. Schroeder, 1991: The New Year's Eve flood on Oahu, Hawaii, December 31, 1987–January 1, 1988. *Natural Disaster Studies,* Vol. 1, National Academy Press, 72 pp.

Dudhia, J., 1989: Numerical study of convection observed during the Winter Monsoon Experiment using a mesoscale two-dimensional model. *J. Atmos. Sci.,* **46,** 3077–3107.

Ek, M. B., K. E. Mitchell, Y. Lin, E. Rogers, P. Grunmann, V. Koren, G. Gayno, and J. D. Tarpley, 2003: Implementation of Noah land surface model advances in the National Centers for Environmental Prediction operational mesoscale Eta Model. *J. Geophys. Res.,* **108,** 8851, doi:10.1029/2002JD003296.

Fankhauser, J. C., 1964: On the motion and predictability of convective systems as related to the upper winds in a case of small turning of wind with height. NSSP Rep. 21, 36 pp.

Frank, W. M., 1978: The life cycle of GATE convective systems. *J. Atmos. Sci.,* **35,** 1256–1264.

Fullerton, C. M., and S. K. Wilson, 1975: An analysis of four showers with rainfall rates > 250 mm/hr. Water Resource Research Center Tech Rep. 90, University of Hawaii at Manoa, 45 pp. [Available from Water Resources Research Center, University of Hawaii at Manoa, Honolulu, HI 96822.]

Fulton, R. A., 1999: Sensitivity of WSR-88D rainfall estimates to the rain-rate threshold and rain gauge adjustment: A flash flood case study. *Wea. Forecasting,* **14,** 604–624.

——, J. P. Breidenbach, D.-J. Seo, D. A. Miller, and T. O'Bannon, 1998: The WSR-88D rainfall algorithm. *Wea. Forecasting,* **13,** 377–395.

George, J. J., 1960: *Weather Forecasting for Aeronautics*. Academic Press, 673 pp.

Giambelluca, T. W., R. E. Martin, G. P. Asner, M. Huang, R. G. Mudd, M. A. Nullet, J. K. DeLay, and D. Foote, 2009: Evapotranspiration and energy balance of native wet montane cloud forest in Hawai'i. *Agric. For. Meteor.,* **149,** 230–243.

Haraguchi, P., 1977: Forecasting floods in Hawaii (excluding Hawaii island). NOAA Tech. Memo. NWSTM PR-16, 30 pp.

Heymsfield, A. J., P. N. Johnson, and J. E. Dye, 1978: Observations of moist adiabatic ascent in northeast Colorado cumulus congestus clouds. *J. Atmos. Sci.,* **35,** 1689–1703.

Hong, S.-Y., Y. Noh, and J. Dudhia, 2006: A new vertical diffusion package with an explicit treatment of entrainment processes. *Mon. Wea. Rev.,* **134,** 2318–2341.

Janjic, Z. I., 1994: The step-mountain eta coordinate model: Further developments of the convection, viscous sublayer and turbulence closure schemes. *Mon. Wea. Rev.,* **122,** 927–945.

Kain, J. S., and J. M. Fritsch, 1993: Convective parameterization in mesoscale models: The Kain–Fritsch scheme. *The Representation of Cumulus Convection in Numerical Models, Meteor. Monogr.,* No. 46, Amer. Meteor. Soc., 165–170.

Khain, A. P., A. Pokrovsky, M. Pinsky, A. Seifert, and V. Phillips, 2004: Simulation of effects of atmospheric aerosols on deep turbulent convective clouds using a spectral microphysics mixed-phase cumulus cloud model. Part I: Model description and possible applications. *J. Atmos. Sci.,* **61,** 2963–2982.

Knight, N. C., 1981: The climatology of hailstone embryos. *J. Appl. Meteor.,* **20,** 750–755.

Kodama, K., and G. M. Barnes, 1997: Heavy rain events over the south-facing slopes of Hawaii: Attendant conditions. *Wea. Forecasting,* **12,** 347–367.

——, and S. Businger, 1998: Weather and forecasting challenges in the Pacific region of the National Weather Service. *Wea. Forecasting,* **13,** 253–276.

Leopold, L. B., 1949: The interaction of trade wind and sea breeze, Hawaii. *J. Meteor.,* **6,** 312–320.

Lin, Y.-L., R. D. Farley, and H. D. Orville, 1983: Bulk parameterization of the snow field in a cloud model. *J. Climate Appl. Meteor.,* **22,** 1065–1092.

——, S. Chiao, T.-A. Wang, M. L. Kaplan, and R. P. Weglarz, 2001: Some common ingredients for heavy orographic rainfall. *Wea. Forecasting,* **16,** 633–660.

Ludlam, F. H., 1963: Severe local storms: A review. *Severe Local Storms, Meteor. Monogr.,* No. 27, Amer. Meteor. Soc., 1–30.

Lyman, R. E., T. A. Schroeder, and G. M. Barnes, 2005: The heavy rain event of 29 October 2000 in Hana, Maui. *Wea. Forecasting,* **20,** 397–414.

Macdonald, G. A., A. T. Abbot, and F. L. Peterson, 1983: *Volcanoes in the Sea: The Geology of Hawaii*. University of Hawaii Press, 517 pp.

Maddox, R. A., C. F. Chappell, and L. R. Hoxit, 1979: Synoptic and meso-alpha scale aspects of flash flood events. *Bull. Amer. Meteor. Soc.,* **60,** 115–123.

Mlawer, E. J., S. J. Taubman, P. D. Brown, M. J. Iacono, and S. A. Clough, 1997: Radiative transfer for inhomogeneous atmosphere: RRTM, a validated correlated-k model for the long-wave. *J. Geophys. Res.,* **102** (D14), 16 663–16 682.

Nair, U. S., H. R. Mark, and R. A. Pielke Sr., 1997: Numerical simulation of the 9–10 June 1972 Black Hills storm using CSU RAMS. *Mon. Wea. Rev.,* **125,** 1753–1766.

Nash, A., N. Rydell, and K. Kodama, cited 2009: Unprecedented extended wet period across Hawaii—February 19 to April 2, 2006. [Available online at http://www.prh.noaa.gov/hnl/pages/events/weeksrain/weeksrainsummary.php.]

Newton, C. W., 1966: Circulations of large sheared cumulonimbus. *Tellus,* **18,** 699–713.

Pereyra, R. G., E. E. Avila, N. E. Castellano, and C. P. R. Saunders, 2000: A laboratory study of graupel charging. *J. Geophys. Res.,* **105,** 20 803–20 813.

Pessi, A., S. Businger, K. L. Cummins, N. Demetriades, M. Murphy, and B. Pifer, 2009: Development of a long-range lightning detection network for the Pacific: Construction, calibration, and performance. *J. Atmos. Oceanic Technol.,* **26,** 145–166.

Petersen, W. A., and Coauthors, 1999: Mesoscale and radar observations of the Fort Collins flash flood of 28 July 1997. *Bull. Amer. Meteor. Soc.,* **80,** 191–216.

Pflaum, J. C., and H. R. Pruppacher, 1979: A wind tunnel investigation of the growth of graupel initiated from frozen drops. *J. Atmos. Sci.,* **36,** 680–689.

Phillips, V. T. J., A. M. Blyth, P. R. A. Brown, T. W. Choularton, and J. Latham, 2001: The glaciation of a cumulus cloud over New Mexico. *Quart. J. Roy. Meteor. Soc.,* **127,** 1513–1534.

Rotunno, R., J. B. Klemp, and M. L. Weisman, 1988: A theory for strong, long-lived squall lines. *J. Atmos. Sci.,* **45,** 463–485.

Rutledge, S., E. Williams, and T. Keenan, 1992: The Down Under Doppler and Electricity Experiment (DUNDEE): Overview and preliminary results. *Bull. Amer. Meteor. Soc.,* **73,** 3–16.

Saunders, C. P. R., 1993: A review of thunderstorm electrification processes. *J. Appl. Meteor.,* **32,** 642–655.

——, W. D. Keith, and R. P. Mitzeva, 1991: The effect of liquid water content on thunderstorm charging. *J. Geophys. Res.,* **96,** 11 007–11 017.

Schroeder, T. A., 1977: Meteorological analysis of an Oahu flood. *Mon. Wea. Rev.,* **105,** 458–468.

——, 1978: Mesoscale structure of Hawaiian rainstorms. Water Resource Research Center Tech. Rep. 119, University of Hawaii at Manoa, 69 pp.

Skamarock, W. C., and Coauthors, 2008: A description of the Advanced Research WRF version 3. NCAR Tech. Note 475 STR, 113 pp.

Takahashi, T., 1978: Riming electrification as a charge generation mechanism in thunderstorms. *J. Atmos. Sci.,* **35,** 1536–1548.

——, 1987: Hawaiian hailstones—30 January 1985. *Bull. Amer. Meteor. Soc.,* **68,** 1530–1534.

Wang, R., I. P. Wu, and L. S. Lau, 1970: Instantaneous unit hydrograph analysis of Hawaiian small watersheds. Water Resources Research Center Tech. Rep. 42, University of Hawaii at Manoa, 54 pp.

Wapler, K., T. P. Lane, P. T. May, C. Jakob, M. J. Manton, and S. T. Siems, 2010: Cloud-system-resolving model simulations of tropical cloud systems observed during the Tropical Warm Pool-International Cloud Experiment. *Mon. Wea. Rev.,* **138,** 55–73.

Warner, T. T., and H. Hsu, 2000: Nested-model simulation of moist convection: The impact of coarse-grid parameterized convection on fine-grid resolved convection. *Mon. Wea. Rev.,* **128,** 2211–2231.

Weisman, M. L., and J. B. Klemp, 1984: The structure and classification of numerically simulated convective storms in directionally varying wind shears. *Mon. Wea. Rev.,* **112,** 2479–2498.

Williams, E. R., S. A. Rutledge, S. G. Geotis, N. Renno, E. Rasmussen, and T. Rickenbacch, 1992: A radar and electrical study of tropical ''hot towers.'' *J. Atmos. Sci.,* **49,** 1386–1395.

——, V. C. Mushtak, D. Rosenfeld, S. J. Goodman, and D. J. Boccippio, 2005: Thermodynamic conditions favorable to superlative updrafts, mixed phase microphysics and lightning flash rate. *Atmos. Res.,* **76,** 288–306.